

Kinetic Characterization of Xenobiotic Reductase A from *Pseudomonas putida* 86[†]

Olivia Spiegelhauer,[‡] Frank Dickert,[§] Sophia Mende,[‡] Dimitri Niks,^{||} Russ Hille,^{||} Matthias Ullmann,[§] and Holger Dobbek^{*,‡}

[‡]*Bioinorganic Chemistry and* [§]*Structural Biology/Bioinformatics, University of Bayreuth, 95447 Bayreuth, Germany, and* ^{||}*Department of Biochemistry, University of California, Riverside, California 92507*

Received August 6, 2009; Revised Manuscript Received September 25, 2009

ABSTRACT: Xenobiotic reductase A (XenA) from *Pseudomonas putida* is a member of the old-yellow-enzyme family of flavin-containing enzymes and catalyzes the NADH/NADPH-dependent reduction of various substrates, including 8-hydroxycoumarin and 2-cyclohexenone. Here we present a kinetic and thermodynamic analysis of XenA. In the reductive half-reaction, complexes of oxidized XenA with NADH or NADPH form charge-transfer (CT) intermediates with increased absorption around 520–560 nm, which occurs with a second-order rate constant of $9.4 \times 10^5 \text{ M}^{-1} \text{ s}^{-1}$ with NADH and $6.4 \times 10^5 \text{ M}^{-1} \text{ s}^{-1}$ with NADPH, while its disappearance is controlled by a rate constant of 210–250 s^{-1} with both substrates. Transfer of hydride from NADPH proceeds 24 times more rapidly than from NADH. This modest kinetic preference of XenA for NADPH is unlike the typical discrimination between NADH and NADPH by binding affinity. Docking studies combined with electrostatic energy calculations indicate that the 2'-phosphate group attached to the adenine moiety of NADPH is responsible for this difference. The reductions of 2-cyclohexenone and coumarin in the oxidative half-reaction are both concentration-dependent under the assay conditions and reveal a more than 50-fold larger limiting rate constant for the reduction of 2-cyclohexenone compared to that of coumarin. Our work corroborates the link between XenA and other members of the old-yellow-enzyme family but demonstrates several differences in the reactivity of these enzymes.

Xenobiotic reductases are bacterial enzymes of the old-yellow-enzyme (OYE)¹ family known to catalyze the reduction of the olefinic bond of α,β -unsaturated carbonyl compounds, including ketones and esters with NADH or NADPH as the electron source (1–7). Xenobiotic reductase A (XenA) from *Pseudomonas putida* catalyzes the NAD(P)H-dependent reduction of various biotic and abiotic compounds (8). Recently, it was shown that XenA catalyzes the reduction of the C3–C4 double bond of 8-hydroxycoumarin, indicating its involvement in the degradation of quinoline, a ubiquitous N-heterocyclic pollutant with carcinogenic properties (9), along the 8-hydroxycoumarin pathway in *P. putida* 86 (10).

The crystal structure of XenA has been determined for the enzyme alone and in complex with two different substrates (10). The structure reveals a dimeric arrangement with one (β/α)₈ barrel domain per monomer, which binds a FMN molecule on the solvent-exposed C-terminal side of the barrel. A tryptophan residue from the C-terminal helix of the neighboring monomer protrudes into the active site and forms one wall of the substrate-binding pocket. The active site is further lined by histidine and tyrosine residues, which presumably are needed to bind and orient the substrates, stabilize developing charges during

turnover, and donate protons. A feature distinguishing XenA from most members of the OYE family is the presence of a cysteine residue in the active site near the N5 position of the isoalloxazine ring (10). XenA shares its overall arrangement and active site architecture with YqjM, and both have been suggested to form a new subfamily within the OYE family (11).

Genome sequencing projects revealed the OYE-like enzymes to be a rapidly growing family, which in some organisms, such as *Saccharomyces cerevisiae* (12), *Shewanella oneidensis* (13), and *P. putida* KT2440 (14), occur in up to six copies. The modest substrate specificity of OYE-like enzymes has attracted the attention of biotechnologists (15), further motivating more detailed studies of the physiological function and catalytic mechanisms of different variants. Therefore, several members of this enzyme family have been intensely studied, and the structural, kinetic, and thermodynamic characteristics of their interaction with various substrates have been elucidated, which have revealed that despite their similar structures they differ remarkably in their reactivities (11, 16–33). Here, we have investigated the thermodynamic characteristics of XenA and studied its reactivity with various substrates. Our data suggest an electrostatic basis for the kinetic preference of XenA for NADPH over NADH.

EXPERIMENTAL PROCEDURES

Chemicals and Enzymes. Complex microbial media were purchased from Roth and Otto Nordwald and were prepared as described by Sambrook et al. (35). All chemicals and enzymes were purchased from Fluka and AppliChem. 5-Deaza-10-methyl-3-sulfopropylisoalloxazine was a gift from P. M. H. Kroneck (University of Konstanz, Konstanz, Germany). The extinction

[†]This work was funded by grants from the Deutsche Forschungsgemeinschaft (DFG, DO-785/2), the Fonds der chemischen Industrie, and the Bavarian-Californian Technology Centre.

*To whom correspondence should be addressed: Universitätsstrasse 30, 95440 Bayreuth, Universität Bayreuth, Germany. Telephone: (+49) 921-554364. Fax: (+49) 921-552432. E-mail: Holger.Dobbek@unj-bayreuth.de.

Abbreviations: CT, charge transfer; EDTA, ethylenediaminetetraacetate; FMN, flavin mononucleotide; OYE, old yellow enzyme; PDB, Protein Data Bank; XenA, xenobiotic reductase A.

coefficients of XenA ($\epsilon_{280} = 71050 \text{ M}^{-1} \text{ cm}^{-1}$, and $\epsilon_{464} = 12200 \text{ M}^{-1} \text{ cm}^{-1}$), NADH ($\epsilon_{340} = 6200 \text{ M}^{-1} \text{ cm}^{-1}$), and NADPH ($\epsilon_{340} = 6220 \text{ M}^{-1} \text{ cm}^{-1}$) were used to calculate the concentrations of the enzyme, cofactor, and substrates.

Protein Expression, Purification, and Activity Assay. The gene of XenA was isolated from *P. putida* 86 and cloned into a pET11a vector as described previously (10). XenA was expressed in *Escherichia coli* Rosetta(DE3)pLysS using LB medium supplemented with 100 $\mu\text{g}/\text{mL}$ ampicillin and 34 $\mu\text{g}/\text{mL}$ chloramphenicol, at 20 °C overnight.

Crude cell extracts were prepared in 50 mM Tris buffer (pH 8.0) for a purification that included three chromatographic steps. The first column was a Q-Sepharose FF column, followed by Source 15-ISO and Sephacryl S-200 columns. Before size-exclusion chromatography was conducted, the protein was reconstituted on ice with 5 mM FMN overnight. Eight liters of cell culture yielded 600 mg of enzyme with a purity exceeding 95% estimated via SDS-PAGE (data not shown). The pure enzyme was stored at a concentration of $\sim 50 \text{ mg}/\text{mL}$ in 50 mM Tris buffer (pH 8.0) at $-80 \text{ }^\circ\text{C}$.

The specific activity of XenA was determined from absorbance changes at 340 nm due to the oxidation of NADPH. To prevent the oxidase activity of XenA, all kinetic measurements were performed under anoxic conditions. We made solutions anoxic by bubbling them with dinitrogen gas. The cuvettes were sealed by screw caps with a rubber septum and flushed with dinitrogen gas before use. The typical oxidase activity found under these conditions was 0.14 unit mg^{-1} . Activity tests were performed using an Analytik Jena Specord40 spectrophotometer at 25 °C. The reaction mixture contained 50 mM Tris-HCl (pH 8.0), 300 μM 2-cyclohexenone, and 150 μM NADPH. The reaction was started by addition of enzyme to the reaction mixture and conducted in a volume of 1 mL with a XenA concentration of approximately $1 \times 10^{-2} \text{ mg mL}^{-1}$. One activity unit is defined as the oxidation of 1 μmol of NADPH/min.

We determined the flavin content spectrophotometrically by SDS treatment according to the protocol by Aliverti et al. (36).

Photoreduction of XenA. Photoreduction of XenA was essentially conducted as described by Massey et al. (37). XenA was photoreduced in a glass tonometer with a cuvette attached to a side arm. As a photoreductant, we used the potassium salt of 5-deaza-10-methyl-3-sulfopropylisoalloxazine, a deazaflavin derivative, in catalytic amounts. The cuvette contained 5-deaza-10-methyl-3-sulfopropylisoalloxazine and EDTA in 100 mM Tris buffer (pH 8.0) in a final volume of 1 mL. The tonometer contained XenA and phenosafranine in 100 mM Tris buffer (pH 8.0) in a final volume of 2 mL. Oxygen was removed by repeated evacuation and flushing with dinitrogen gas. After oxygen removal, the two volumes were mixed, resulting in final concentrations of 15 mM EDTA, 30 μM XenA, and 1 μM phenosafranine. For illumination, a 100 W lamp from a slide projector (Agfa, Opticus 100) was used. The reduction of XenA was followed by recording absorption spectra directly after and 3 min after each illumination.

Determination of Reduction Potentials. Determination of the reduction potential of XenA-bound FMN in the presence and absence of 1 mM NAD^+ was conducted as described previously (38). The reaction mixture contained 15 μM XenA, 15 μM phenosafranine [$E_{\text{m,D}}^\circ = -252 \text{ mV}$ (39)] as a reference dye, 2 μM methylviologen as an electron mediator, and 0.05 unit of xanthine oxidase. The reaction was conducted under anaerobic conditions in a glass tonometer and started by addition of

xanthine with a final concentration of 300 μM . To calculate the concentrations of oxidized XenA (E_{ox}) and oxidized phenosafranine (D_{ox}), the absorbance values at 464 and 521 nm were used and integrated in eqs 1 and 2.

$$A_{464} = \epsilon^{E_{\text{ox}}}{}_{464}c^{E_{\text{ox}}} + \epsilon^{D_{\text{ox}}}{}_{464}c^{D_{\text{ox}}} + \epsilon^{E_{\text{tot}}}{}_{464}(c^{E_{\text{tot}}} - c^{E_{\text{ox}}}) + \epsilon^{D_{\text{red}}}{}_{464}(c^{D_{\text{tot}}} - c^{D_{\text{ox}}}) \quad (1)$$

$$A_{521} = \epsilon^{E_{\text{ox}}}{}_{521}c^{E_{\text{ox}}} + \epsilon^{D_{\text{ox}}}{}_{521}c^{D_{\text{ox}}} + \epsilon^{E_{\text{red}}}{}_{521}(c^{E_{\text{tot}}} - c^{E_{\text{ox}}}) + \epsilon^{D_{\text{red}}}{}_{521}(c^{D_{\text{tot}}} - c^{D_{\text{ox}}}) \quad (2)$$

Following are the values of the molar extinction coefficients: $\epsilon(\text{oxidized enzyme at } 464 \text{ nm}) = 12.2 \times 10^3 \text{ M}^{-1} \text{ cm}^{-1}$, $\epsilon(\text{reduced enzyme at } 464 \text{ nm}) = 0.6 \times 10^3 \text{ M}^{-1} \text{ cm}^{-1}$, $\epsilon(\text{oxidized enzyme at } 521 \text{ nm}) = 1.5 \times 10^3 \text{ M}^{-1} \text{ cm}^{-1}$, $\epsilon(\text{reduced enzyme at } 521 \text{ nm}) = 0.6 \times 10^3 \text{ M}^{-1} \text{ cm}^{-1}$, $\epsilon(\text{oxidized dye at } 464 \text{ nm}) = 12.9 \times 10^3 \text{ M}^{-1} \text{ cm}^{-1}$, $\epsilon(\text{reduced dye at } 464 \text{ nm}) = 0.3 \times 10^3 \text{ M}^{-1} \text{ cm}^{-1}$, $\epsilon(\text{oxidized dye at } 521 \text{ nm}) = 44.9 \times 10^3 \text{ M}^{-1} \text{ cm}^{-1}$, and $\epsilon(\text{reduced dye at } 521 \text{ nm}) = 0.3 \times 10^3 \text{ M}^{-1} \text{ cm}^{-1}$.

The reduction potential of XenA ($E_{\text{m,E}}^\circ$) can subsequently be determined from the difference (ΔE°) in the reduction potentials of the enzyme and dye. The latter can be obtained from the plot of $\log(E_{\text{ox}}/E_{\text{red}})$ versus $\log(D_{\text{ox}}/D_{\text{red}})$ using eq 3.

$$E_{\text{m,E}}^\circ = E_{\text{m,D}}^\circ + \Delta E^\circ \quad (3)$$

Steady-State Kinetics Experiments. The steady-state kinetics of XenA reacting with various concentrations of 2-cyclohexenone and NADPH were performed under anaerobic conditions. The concentration of 2-cyclohexenone was varied between 10 and 160 μM , and the concentration of NADPH was varied between 10 and 400 μM . Each single measurement was performed three times. 2-Cyclohexenone and NADPH were both added from a freshly prepared 1 mM stock solution, and the concentration of XenA was approximately 250 nM. The apparent values for $K_{\text{m,A}}$, $K_{\text{m,B}}$, and V_{max} have been determined by multiple nonlinear regression analysis of the measured rates using eq 4 (40):

$$v = \frac{V_{\text{max}}[A][B]}{K_{\text{m,B}}[A] + K_{\text{m,A}}[B] + [A][B]} \quad (4)$$

where [A] is the concentration of 2-cyclohexenone, [B] is the concentration of NADPH, v is the observed rate, V_{max} is the rate at saturating substrate concentrations, $K_{\text{m,A}}$ is the K_{m} for 2-cyclohexenone at saturating NADPH levels, and $K_{\text{m,B}}$ is the K_{m} for NADPH at saturating 2-cyclohexenone levels.

Rapid Reaction Techniques. Measurements on the kinetics of the reductive half-reaction were performed under anaerobic conditions using an Applied Photophysics SX-20MV kinetic spectrophotometer with a 1 cm observation path length cuvette coupled either to a diode array detector or to a monochromator and photomultiplier. The reaction temperature was controlled with a Haake F8/C25 thermostat. Standard reaction conditions were 50 mM Tris (pH 8.0) at 20 °C. In a typical experiment, enzyme at a XenA concentration of approximately 10 μM was mixed with an equal volume of substrate solution, the latter at concentrations ranging from 50 to 5000 μM . Each experiment was repeated at least five times for each substrate concentration. The reactions were monitored at 464 and 540 nm over an appropriate time scale. Observed kinetic transients at 464 nm were fit to single exponentials, and transients at 540 nm,

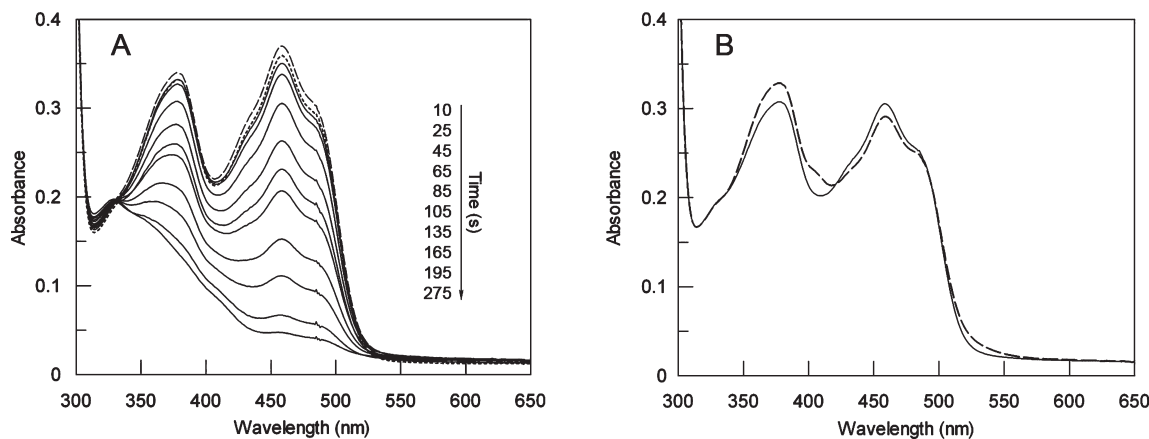
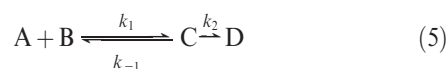


FIGURE 1: Photoreduction of XenA. Conditions: 30 μ M XenA, 15 mM EDTA, 1 μ M phenosafranine, 100 mM Tris buffer (pH 8.0), and traces of 5-deaza-10-methyl-3-sulfolpropylisoalloxazine as catalyst. (A) Time-dependent reduction of XenA after illumination. The figure shows the spectra recorded before (\cdots) and after (—) different periods of illumination. The spectrum of reoxidized XenA is displayed as a dashed line. (B) Spectra recorded directly (---) and 3 min (—) after a single irradiation step.

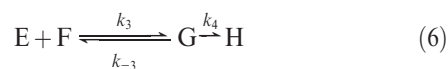
monitoring formation and decay of charge-transfer complexes, were fit with double exponentials using Pro-Data (Applied Photophysics) to yield observed rate constants (k_{obs}).

The reductive half-reaction sequence was modeled as shown in eq 5



where A is XenA_{ox}, B is NAD(P)H, C is the XenA–NAD(P)H charge-transfer complex, and D is XenA containing the two-electron-reduced state of FMN and bound NAD(P)⁺.

The oxidative half-reaction sequence was modeled as shown in the general eq 6



where E is XenA_{red}, F is 2-cyclohexenone (coumarin), G is the XenA_{red}–2-cyclohexenone (coumarin) charge-transfer complex, and H is XenA_{ox} with bound 2-cyclohexanone (chroman-2-one).

Hyperbolic plots of observed rate constants versus substrate concentration were fitted using eq 7 to yield the limiting rate of reaction at high [S], k_X , and the dissociation constant K_D (41).

$$k_{\text{obs}} = k_X[S]/(K_D + [S]) \quad (7)$$

$$k_{\text{obs}} = k_1[S] + k_{-1} + k_2 \quad (8)$$

Rate constants for the formation of the charge-transfer complex between oxidized XenA and NADH/NADPH were approximated by linear regression analysis with eq 8, where k_2 is the limiting rate of reduction of XenA with the respective nicotinamide used.

To relate the individual limiting rate constants of the reductive and oxidative half-reactions to the steady-state catalytic constants, eq 9 has been used:

$$k_{\text{cat}} = k_2 k_4 / (k_2 + k_4) = k_{\text{red}} k_{\text{ox}} / (k_{\text{red}} + k_{\text{ox}}) \quad (9)$$

Solutions of oxidized XenA were made anoxic in a glass tonometer as described above. Solutions of reduced XenA were made anoxic in a tonometer with a cuvette side arm and titrated with NADH to achieve complete flavin reduction. We made all substrate solutions anoxic by flushing them with dinitrogen gas.

Docking. NADPH was docked to the crystal structure of XenA (PDB entry 2H8X) using DOCK 6 (42). The charges were taken from the CHARMM27 force field (43). A “divide and conquer” approach was used to reduce the number of rotatable bonds. The nicotinamide was docked close to FMN using chemical docking, which was used to incorporate information about the chemical complementarity of ligand and receptor moieties into the matching process. In a second step, adenosine was independently docked within a radius of 25 Å from FMN. The remaining parts of NAD(P)H (i.e., the ribose and phosphates) were constructed geometrically and subsequently energetically minimized using CHARMM (44), while the rest of the protein, the nicotinamide ring and the adenine ring, was kept fixed.

Electrostatic Calculations. To study the effects of the phosphate group of NADPH on the hydride-transfer energies between the nicotinamide ring and the isoalloxazine ring, electrostatics were calculated using the program SOLINPROT of the MEAD package (45). We calculated the interaction of the nicotinamide ring and the isoalloxazine ring with the monophosphate group bound to the ribose before and after the electron transfer. The XenA dimer was used to define the dielectric boundaries. For this calculation, only the charges of the nicotinamide ring and the phosphate group of NADPH and the isoalloxazine ring of the FMN were considered. The dielectric constants of protein and of water were set to 4.0 and 80.0, respectively. The ionic strength was set to 0.1 M. The calculation was done in two focusing levels with grids of 181 \times 180 \times 180 grid points. The grid spacing was set to 1.0 and 0.25 Å for the outer and the inner grid, respectively. The outer grid was centered at the coordinate center of the protein; the inner grid was centered at the N1 atom of FMN.

RESULTS

Photoreduction of XenA. XenA was reduced using the light-mediated generation of electrons by the deazaflavin–EDTA couple in the presence of phenosafranine as the redox mediator (Figure 1A). This method has been applied to ensure single electron transfer to allow for initial semiquinone formation. Photoreduction proceeds in a two-step mechanism. Directly after each illumination period, we observe a signal increase around 350 nm, which we assign to the formation of the red anionic

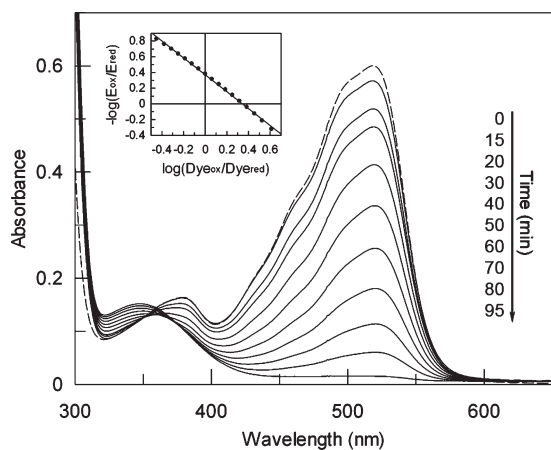


FIGURE 2: Redox potential determination for the FMN-FMNH⁻ couple of XenA. Conditions: 15 μ M XenA, 15 μ M phenosafranin, 2 μ M methylviologen, 0.05 unit of xanthine oxidase, and 50 mM Tris buffer (pH 8.0). The dotted line shows the spectrum of the reaction mixture before the addition of xanthine. The reaction was followed over 1.5 h (—). Absorbance values at 464 and 521 nm were used to calculate the concentrations of oxidized XenA and the dye. The inset shows the plot of $\log(E_{\text{ox}}/E_{\text{red}})$ vs $\log(D_{\text{ox}}/D_{\text{red}})$. The solid line displays the linear fit with a slope of -1 . The redox potential of XenA was calculated to be -263 mV.

semiquinone. Figure 1B shows the spectrum (dashed line) with a characteristic peak around 400 nm and an increase in signal magnitude between 500 and 550 nm. Three minutes after illumination, the semiquinone signature was not observed any more and the enzyme-bound flavin was converted to the dihydroflavin form as a result of the dismutation of the semiquinone. After complete reduction of the enzyme, the cuvette was exposed to air, allowing XenA to reoxidize, resulting in a spectrum indistinguishable from the starting spectrum.

Determination of Reduction Potential. The generation of electrons by the xanthine oxidase-xanthine couple has been used as an alternative method to reduce XenA. The presence of a reference dye (phenosafranin; $E^{\circ}_{\text{m}} = -252$ mV) allowed the determination of the reduction potential of XenA-bound FMN. The small amount of xanthine oxidase ensured equilibrium conditions at all times, whereas both enzyme and dye take up two electrons. Reduction of XenA by xanthine oxidase in the absence of phenosafranin showed the slow conversion of FMN from the quinone to the hydroquinone state without any detectable formation of semiquinone species (data not shown). Spectra recorded during the reaction with phenosafranin show that XenA and phenosafranin are reduced to similar extents (Figure 2). The absorbance values at 464 and 521 nm were used to calculate the amount of oxidized XenA and dye using eqs 1 and 2. Equation 3 gives a reduction potential of -263 mV for XenA. The linear fit of the plot of $\log(E_{\text{ox}}/E_{\text{red}})$ versus $\log(D_{\text{ox}}/D_{\text{red}})$ shows a slope of -1 , confirming that both XenA and phenosafranin received the same amount of electrons and reacted under equilibrium conditions. There was no difference observed in the presence of 1 mM NAD^+ and 1 mM NADP^+ .

Steady-State Kinetics. Catalytic turnover of XenA with various concentrations of 2-cyclohexenone and NADPH under anaerobic conditions was analyzed to determine the values of K_{mA} , K_{mB} , and V_{max} . The inset in Figure 3 shows the rate dependencies of 2-cyclohexenone for different NADPH concentrations and the corresponding nonlinear fits using the normal Michaelis-Menten equation. The parallel lines in the double-reciprocal plot

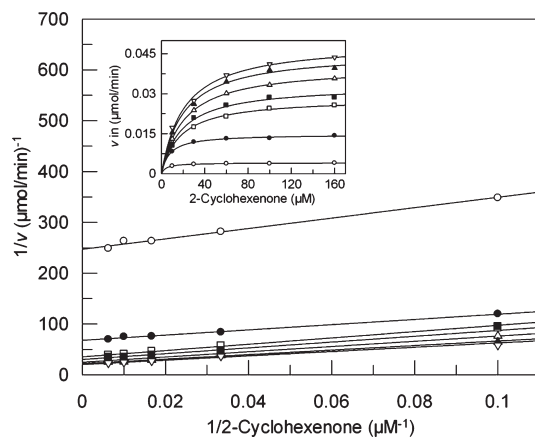


FIGURE 3: Steady-state kinetic data of the XenA-catalyzed reduction of 2-cyclohexenone by NADPH. Lineweaver-Burk plot with linear regression analysis using the simple Michaelis-Menten equation. Each point represents the mean of three independent measurements. The assays were performed in 50 mM Tris buffer (pH 8.0) at 25 $^{\circ}\text{C}$. The final volume of 1 mL contained 250 nM XenA, varying concentrations of 2-cyclohexenone (10–160 μ M), and varying concentrations of NADPH (10–400 μ M). Each line displays one distinct NADPH concentration: (\circ) 10 μ M NADPH, (\bullet) 50 μ M NADPH, (\square) 100 μ M NADPH, (\blacksquare) 150 μ M NADPH, (\triangle) 200 μ M NADPH, (\blacktriangle) 300 μ M NADPH, and (∇) 400 μ M NADPH. The inset displays the direct rate dependencies of 2-cyclohexenone for the different NADPH concentrations (see above) and the nonlinear fits using the simple Michaelis-Menten equation.

(Figure 3) are consistent with a double-displacement (ping-pong) mechanism (40). Consequently, the measured rates were analyzed by multiple nonlinear regression analysis using eq 4, resulting in the following values: $k_{\text{cat}} = 7.2 \pm 0.3$ s^{-1} , K_{mA} (the K_{m} for 2-cyclohexenone) = 37.2 ± 2.4 μ M, and K_{mB} (the K_{m} for NADPH) = 200 ± 13.0 μ M.

Reductive Half-Reaction. The reaction of XenA with NADH and NADPH was next examined following the spectral change associated with reduction of the enzyme's flavin (Figure 4A). No spectral changes indicating the formation of a Michaelis complex in the dead time of the stopped-flow experiment were observed (Figure 4A). Formation of a CT complex, on the other hand, can be discerned by an absorption increase at 520–560 nm (Figure 4B, inset), which decays with a rate constant comparable to that of FMN reduction recorded at 464 nm (Figure 4B). The characteristic absorption around 464 nm shows that the weak CT complex is indeed formed between oxidized XenA and the NADH or NADPH and is not a complex of the reduced enzyme (Figure 4A). The observed rate constant for the formation of the CT complex depends linearly on the concentration of NADH or NADPH (Figure 4C). Using eq 8 to fit the observed dependence of observed rate constants on the concentration of NAD(P)H under pseudo-first-order conditions gives a second-order rate constant (k_1) of $(9.4 \pm 0.5) \times 10^5$ $\text{M}^{-1} \text{s}^{-1}$ with NADH and $(6.4 \pm 0.3) \times 10^5$ $\text{M}^{-1} \text{s}^{-1}$ with NADPH for the formation of the CT complex. The rate constants for the dissociation of NAD(P)H from the CT complex (k_{-1}) have been derived from the positive intercept on the ordinate, which is approximated to be $k_{-1} + k_2$. The values for k_{-1} are very similar for both nicotinamides with 256 ± 17 s^{-1} for NADH and 215 ± 11 s^{-1} for NADPH. The rate constants determined for the decay of the CT complex at long wavelengths (Figure 4B, inset) correspond to the observed rates measured for the reduction of FMN seen at 464 nm and show a hyperbolic dependence on the concentration of reduced nicotinamide (Figure 4D,E). The linear

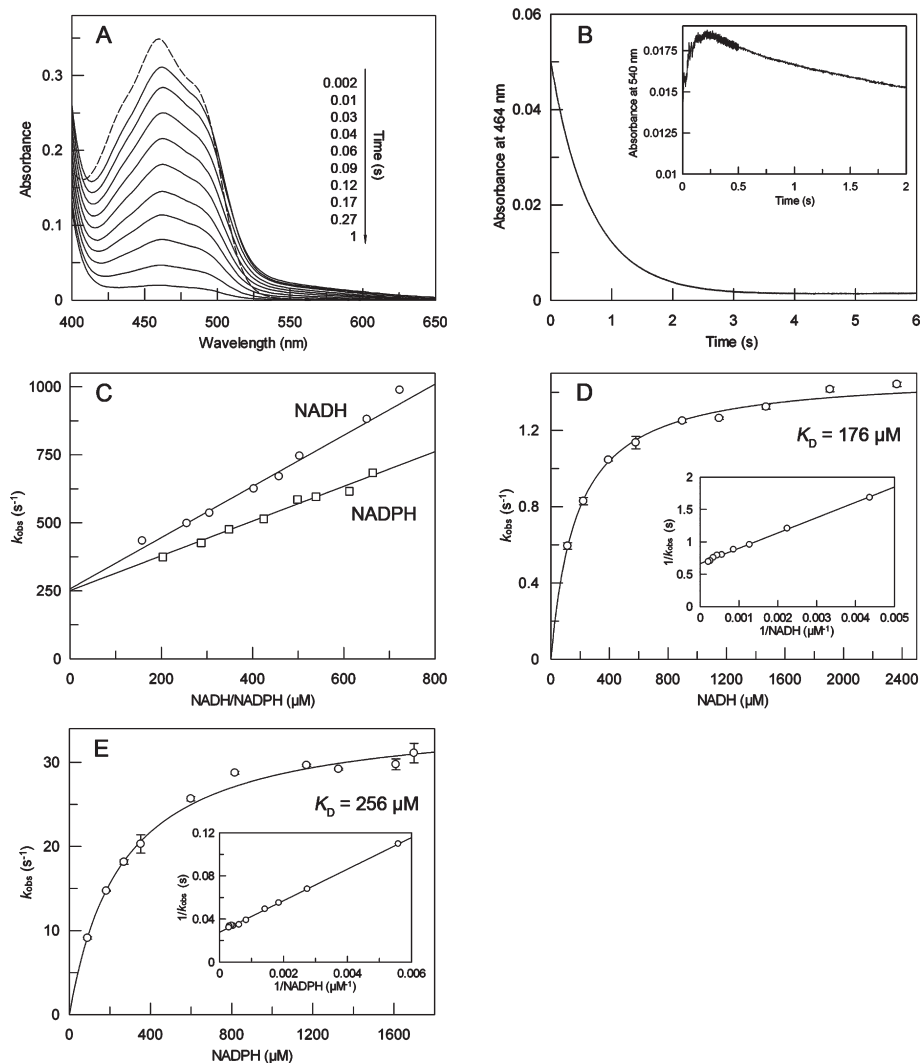


FIGURE 4: Reductive half-reactions of XenA with NADH and NADPH. (A) Time-dependent spectral changes of 35 μM XenA_{ox} reacting with 800 μM NADH (corresponding to 70 μM XenA_{ox} and 1600 μM NADH before mixing). The dashed line represents the spectrum of XenA_{ox}. (B) Time-dependent absorbance change at 464 nm for the reaction of 5 μM XenA with 2500 μM NADH. The inset displays the absorbance changes at 540 nm (with 35 μM XenA and 50 μM NADH), which we attribute to the formation of the CT complex. (C) Dependencies of the observed rates at 540 nm (CT formation) on NADH concentration (O) and NADPH concentration (□) for reactions with 35 μM XenA. (D and E) Concentration dependence of the observed rates at 464 nm (5 μM XenA) for NADH (D) and NADPH (E), with the reciprocal plots in the insets. The curves display the best fits to the data using eq 7. All experiments were conducted under anaerobic conditions in 50 mM Tris buffer (pH 8.0) at 20 °C.

correlation of $1/k_{\text{obs}}$ with $1/[\text{NADH}]$ or $1/[\text{NADPH}]$ (Figure 4D, E, insets) indicates that the equilibrium condition for the XenA–NAD(P)H reaction ($k_{-1} \gg k_2$) holds, as seen experimentally, and that eq 7 can be used to determine the limiting rate constant for the reduction of FMN (k_2) and the dissociation constant (K_D) of the complex (41). For the reaction of XenA_{ox} with NADH, a rate constant (k_2) of $1.50 \pm 0.02 \text{ s}^{-1}$ is obtained, while with NADPH, the rate constant is 24 times higher, $35.7 \pm 0.6 \text{ s}^{-1}$. The dissociation constants for the XenA_{ox}–NADH complex of $176 \pm 14 \mu\text{M}$ and for the XenA_{ox}–NADPH complex of $256 \pm 12 \mu\text{M}$ obtained using the rapid equilibrium model are in good agreement with the ratio between the rate constants for the formation of the CT complexes (XenA_{ox}–NADH, $k_{-1}/k_1 = 272 \mu\text{M}$; XenA_{ox}–NADPH, $k_{-1}/k_1 = 336 \mu\text{M}$). Appreciable rates for the back reaction would cause the double-reciprocal plot of $1/k_{\text{obs}}$ versus $1/[\text{NAD(P)H}]$ to curve down for high substrate concentrations (41), which is not observed (Figure 4D,E, insets). Furthermore, an adaptation of the model to include the rate constant of the back-reaction (k_{-2}) did not improve the fit to the observed rates, as judged from testing the goodness of fit. We

conclude that k_{-2} is very small and that reduction of XenA by either NADH or NADPH is functionally irreversible.

Oxidative Half-Reaction. To examine the reoxidation of XenA, two different substrates have been studied, 2-cyclohexenone and coumarin. 2-Cyclohexenone has been used as a substrate in most rapid kinetic studies with members of the OYE family, notably with OYE (19), morphinone reductase (24, 46), PETN reductase (29), and YqjM (34), and it is therefore possible to compare the reactivity of XenA with the reactivities of these enzymes. However, since we have recently shown that XenA participates in the degradation of quinoline along the 8-hydroxycoumarin pathway and is able to reduce the C3–C4 double bonds of heteroaromatic compounds such as coumarin (10), we have also examined the reaction of XenA with this substrate.

Spectral changes are observed directly after reduced XenA reacts with 50 μM 2-cyclohexenone, as compared to the spectrum of reduced XenA with substrate (Figure 5A). The observed maximum at 424 nm 5 ms after reduced XenA is mixed with 2-cyclohexenone indicates that it is not due to a fast reaction

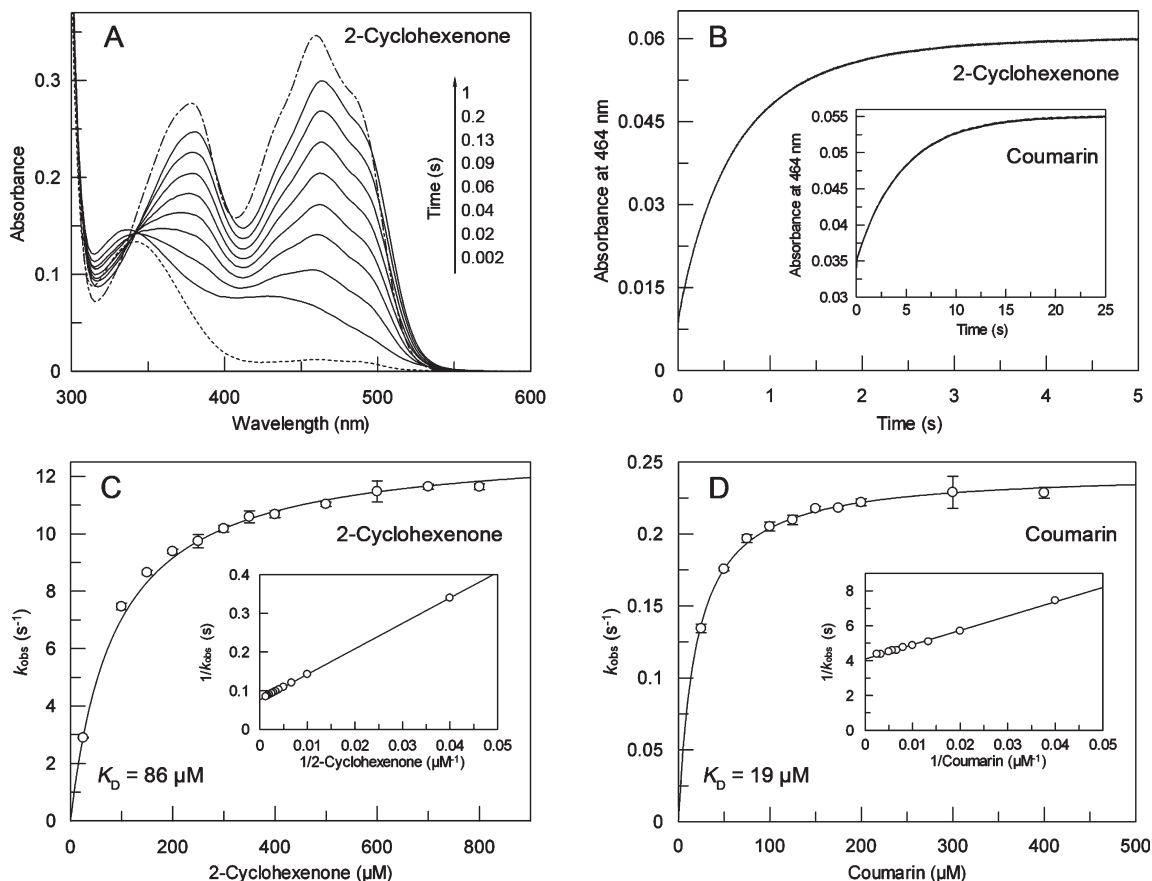


FIGURE 5: Oxidative half-reaction of reduced XenA with 2-cyclohexenone and coumarin. (A) Time-dependent spectral changes of 35 μM XenA (NADH-reduced) reacting with 800 μM 2-cyclohexenone. The dashed line represents the spectrum of reduced XenA. (B) Time-dependent spectral changes at 464 nm for the reaction of 5 μM XenA with 25 μM 2-cyclohexenone. A reaction trace with 25 μM coumarin is shown in the inset of panel B. (C and D) Concentration dependence of the observed rate constants at 464 nm for the reaction of 5 μM XenA with 2-cyclohexenone (C) and for coumarin (D). The curves display the best fits to the data using eq 7. The reciprocal plots are shown in the insets. All experiments were conducted in 50 mM Tris buffer (pH 8.0) at 20 $^{\circ}\text{C}$ under anaerobic conditions.

phase in which FMN is oxidized but rather that another reaction intermediate involving reduced XenA and 2-cyclohexenone is formed rapidly within the dead time of the instrument. Formation of a CT complex is discernible with both substrates by an initial absorption increase around 650 nm (data not shown). The CT complex forms very rapidly and decays with the same rate as XenA becomes oxidized. The low absorbance around 464 nm at very short times indicates that the CT complex involves reduced XenA and substrate. A larger absorption increase is subsequently observed at 464 nm (Figure 5B). The rate constant observed for the majority of the absorbance increase at 464 nm shows a hyperbolic dependence on the concentration of 2-cyclohexenone and coumarin (Figure 5C,D). The linear relation between $1/k_{\text{obs}}$ and $1/[2\text{-cyclohexenone}]$ or $1/[\text{coumarin}]$ (Figure 5C,D, insets) indicates that it is justified to include the rapid equilibrium condition in our model (41). A rate constant (k_4) of $13.1 \pm 0.1 \text{ s}^{-1}$ and a K_D of $86 \pm 2 \mu\text{M}$ have been determined for 2-cyclohexenone. The reduction of coumarin is slower than the reduction of 2-cyclohexenone by a factor of 50 with a rate constant (k_4) of $0.243 \pm 0.001 \text{ s}^{-1}$, and the complex has a K_D of $19.3 \pm 0.2 \mu\text{M}$.

Modeling NADH and NADPH in the Active Site of XenA. We next examined a model for both NADH and NADPH bound to oxidized XenA, generated using the DOCK 6 program. In this model, NADH and NADPH bind both in the same way to XenA. The nicotinamide ring of NAD(P)H docks in a stacked conformation with the isoalloxazine ring of FMN (Figure 6) and is hydrogen-bonded to His178, His181, and

Cys25. The diphosphate forms a salt bridge with Lys106 and a hydrogen bond with Tyr183. The distance between the phosphorus atom of the 2'-phosphate of NADPH and N1 of the nicotinamide is 6.2 \AA . The 2'-phosphate of NADPH is oriented toward the solvent and does not interact with the protein matrix but does form a hydrogen bond to the 2'-OH group of the ribose attached to nicotinamide (Figure 6).

From electrostatic calculations using the Poisson–Boltzmann equation, we find that the free energy of the transfer of hydride from the nicotinamide to the isoalloxazine ring of the FMN is shifted by -1.83 kcal/mol due to the presence of the 2'-phosphate on NADPH compared to NADH. Thus, the hydride transfer is more favorable with NADPH than with NADH. Most of this difference in free energy manifests itself in a lower activation energy for NADPH versus NADH as reflected in the relative limiting rates of reduction (36 s^{-1} vs 1.5 s^{-1} , respectively).

DISCUSSION

Recently, we have shown that XenA participates in the degradation of quinoline and reacts with heteroaromatic compounds such as coumarin and 8-hydroxycoumarin using both NADH and NADPH as electron sources (10). Here we have examined its reactivity with both reducing and oxidizing substrates, allowing us to compare it to related flavoenzymes.

No stable semiquinone form of XenA was observed in the course of the reductive titrations (using either the xanthine–xanthine oxidase or deazaflavin–light couple as the reductant), indicating

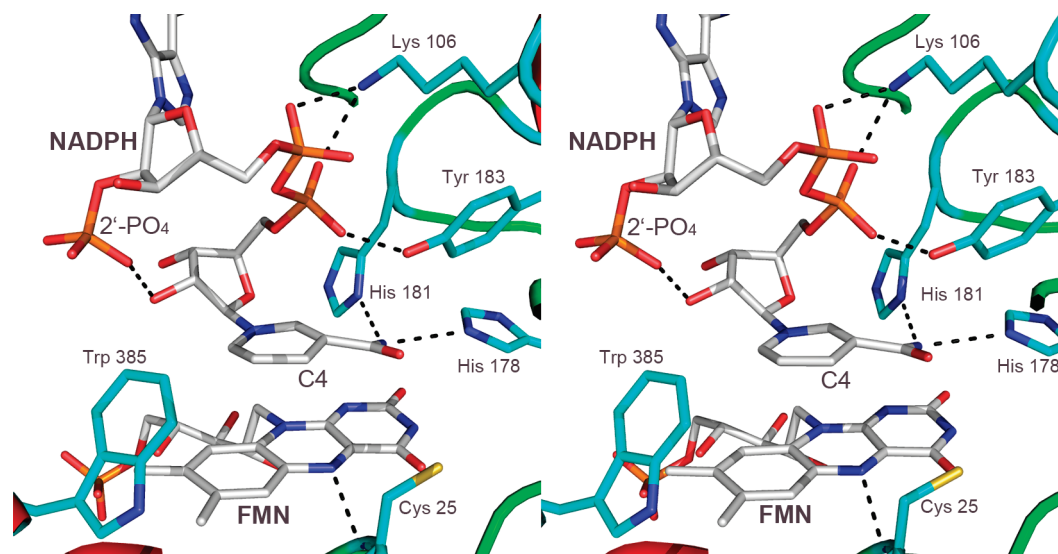


FIGURE 6: Docked complex between XenA and NADPH. The stereoview shows residues of the active site in the vicinity of NADPH depicted as stick models with carbon atoms colored cyan. Interactions mentioned in the text are represented by dashed lines. NADPH and FMN are shown as stick models with carbon atoms colored white. NADH binds to XenA in the same way as NADPH. This figure was generated using PyMol (48).

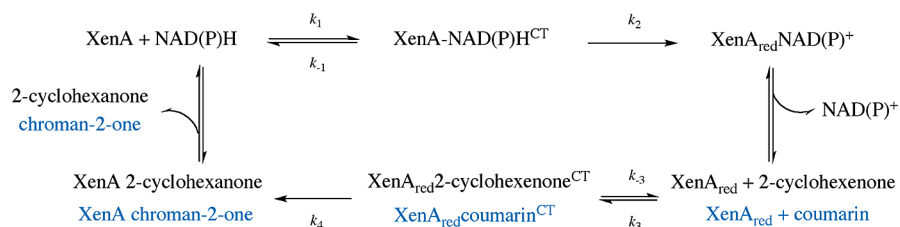


FIGURE 7: Scheme for the reaction cycle catalyzed by XenA.

that transiently formed red, anionic semiquinone rapidly disproportionated. The hydrogen bonding distance between the amide nitrogen of Cys25 and N5 of FMN (Figure 6) indicates that the amide nitrogen acts as hydrogen bond donor and N5 as hydrogen bond acceptor in the oxidized state. This interaction disfavors the formation of the neutral semiquinone as the hydrogen bond would be broken when N5 becomes protonated. The anionic semiquinone is therefore favored; however, as frequently observed, it is thermodynamically unstable. The protein environment thus does not stabilize the semiquinone state to any significant degree. Morphine reductase (24), PETN reductase (29), and YqjM (2) also fail to form detectable amounts of semiquinone, although OYE forms 15–20% of the anionic semiquinone species under equilibrium conditions (47).

The rate constants for the reaction of reductases with both reducing and oxidizing substrates are critically dependent on the reduction potential of the flavin cofactor, which determines which reactions are thermodynamically feasible. The reduction potential of the FMN–FMN^{•−} couple in XenA is −263 mV, substantially lower than found for PETN reductase (−193 mV) (29), OYE (−230 mV) (47), and morphine reductase (−242 mV) (26). XenA has several structural peculiarities that may be responsible for this, including the presence of an active site cysteine residue [Cys25 (Figure 6)] in place of a conserved threonine residue found in other members of the OYE family. The hydroxyl group of the threonine residue of other family members forms a hydrogen bond with the C4 oxygen atom of the isoalloxazine ring, and its replacement with alanine lowered the reduction potential of the FMN–FMN^{•−} couple from −230 to −263 mV in OYE (21) and from −242

to −290 mV in morphine reductase (26). It may therefore be that the presence of the cysteine residue in place of the threonine contributes to the low reduction potential of XenA. We have also examined the reductive and oxidative half-reactions to improve our understanding of the reactivity of XenA. The first observed step in the reductive half-reaction with both NADH and NADPH is the formation of a CT complex. The linear relationship between observed rates of CT complex formation and the concentration of reductants is consistent with a simple bimolecular reaction (Figure 7). There is good agreement between the apparent dissociation constants for the complexes between oxidized XenA and NAD(P)H obtained from the hyperbolic plots of k_{red} versus [NAD(P)H] and the ratio between on and off rate constants for the formation of the CT complexes (k_{-1} and k_1 , respectively, in Figure 6 and Table 1).

To gain further insight into the interaction of NAD(P)H with XenA, we performed docking simulations. In the docked structure, both NADPH and NADH are kept in position by H-bonds to amino acids like His178 and Tyr183, which are highly conserved within the OYE family. The binding mode of NADPH in complex with XenA, including the short distance between the 2'-phosphate and the nicotinamide ring, has not been observed so far. In most flavoprotein structures, the 2'-phosphate is oriented away from the nicotinamide ring and is stabilized by arginine residues.

The second step in the reaction of XenA_{ox} with NAD(P)H is the transfer of hydride from the reduced nicotinamide to the N5 atom of XenA-bound FMN. The rate constants (k_2) for this step differ by a factor of 24 for NADH and NADPH, with the latter being faster. The main difference in the structure of the docked

Table 1: Stopped-Flow Kinetic Data

Reductive Half-Reaction				
substrate	K_d (μM)	k_1 ($\text{M}^{-1} \text{s}^{-1}$)	k_{-1} (s^{-1})	k_2 (s^{-1})
NADH	176 ± 14	$(9.4 \pm 0.5) \times 10^5$	256 ± 17	1.50 ± 0.02
NADPH	256 ± 12	$(6.4 \pm 0.3) \times 10^5$	215 ± 11	35.7 ± 0.6
Oxidative Half-Reaction				
substrate	K_d (μM)	k_4 (s^{-1})		
2-cyclohexenone	86 ± 2	13.1 ± 0.1		
coumarin	19.3 ± 0.6	0.243 ± 0.001		

complexes of NAD(P)H with oxidized XenA is the presence of the 2'-phosphate group, which is situated above the 1,4-dihydropyridine ring of NADPH near the transferred hydrogen at C4. An additional negative charge above the pyridine ring could further stabilize NADP^+ and would therefore be expected to decrease the reduction potential of the $\text{NADP}^+ - \text{NADPH}$ couple in the XenA-bound state. The calculated $\Delta\Delta G$ of -1.83 kcal/mol for the hydride-transfer reaction of XenA-bound NADPH to FMN compared to XenA-bound NADH indicates that the higher rate constant in the reaction with NADPH is due to the interaction of the 2'-phosphate group of NADPH with the nicotinamide ring and the FMN. The lower affinity of XenA for NADPH compared to NADH is more than compensated by its higher reactivity. Using k_2/K_d as a criterion for the specificity of XenA with the two nicotinamides, we obtain apparent second-order rate constants of $8.5 \times 10^3 \text{ M}^{-1} \text{ s}^{-1}$ for NADH and $1.39 \times 10^5 \text{ M}^{-1} \text{ s}^{-1}$ for NADPH, indicating that under physiological conditions XenA reacts preferentially with NADPH. We note that this is an exceptionally low level of selectivity for a flavoprotein. The last step of the reductive half-reaction would be the release of NAD^+ or NADP^+ . We do not observe CT complexes after transfer of hydride to the flavin or any appreciable back-reaction of reduced XenA with NAD^+ or NADP^+ (consistent with the observation that during reductive titrations XenA can be fully reduced with a stoichiometric amount of NADH).

We have also examined the oxidative half-reaction of XenA with 2-cyclohexenone and coumarin. As 2-cyclohexenone is also a substrate of OYE, PETN reductase, and morphinone reductase, we focus our discussion on this substrate. The oxidative half-reaction of the catalytic cycle is initiated by the formation of a CT complex between 2-cyclohexenone and reduced XenA for which the equilibrium dissociation constant could be determined ($86 \mu\text{M}$). Only one intermediate was included in our kinetic model for the oxidative half-reaction, although our data suggest the existence of two different intermediates. The rapid formation of an intermediate in the reaction of reduced OYE and 2-cyclohexenone within the dead time of the stopped-flow spectrophotometer has also been observed, having an absorbance maximum at 455 nm, and was interpreted as a CT complex (19). The observation of two intermediates between reduced XenA and 2-cyclohexenone indicates that their relative orientations are changing from the encounter complex to the reactive complex before the hydride transfer occurs in the fourth step of the reaction. Again we have no indication that an appreciable back-reaction between 2-cyclohexenone and oxidized XenA occurs. The limiting rate constant of the reaction of NADH-reduced XenA with coumarin is 50-fold smaller than that for the reaction

with 2-cyclohexenone, while coumarin binds with a 4-fold higher affinity. The lower reactivity with coumarin probably reflects the weaker electrophilicity of the β -carbon of coumarin compared to 2-cyclohexenone. The good agreement of the catalytic constant derived from eq 4 with NADPH and 2-cyclohexenone as substrates in the steady-state assay ($k_{\text{cat}} = 7.2 \text{ s}^{-1}$) with the catalytic constant following from the limiting rate constants of the reductive and oxidative half-reactions with NADPH and 2-cyclohexenone (eq 9; $k_{\text{cat}} = 5.3 \text{ s}^{-1}$) indicates that the two product release steps, which have not been observed by our transient kinetic analysis, occur rapidly and are not limiting the reaction rate of XenA.

The structures of XenA and other members of the OYE family are very similar, but at the same time, some distinct features in the composition of the active site do exist. This analysis of native XenA revealed further remarkable properties of the enzyme such as its low reduction potential and its only modest specificity for NADPH over NADH.

ACKNOWLEDGMENT

We thank Professor Peter M. H. Kroneck (University of Konstanz) for kindly supplying the deazaflavin derivative.

REFERENCES

- Binks, P. R., French, C. E., Nicklin, S., and Bruce, N. C. (1996) Degradation of pentaerythritol tetranitrate by *Enterobacter cloacae* PB2. *Appl. Environ. Microbiol.* 62, 1214–1219.
- Fitzpatrick, T. B., Amrhein, N., and Macheroux, P. (2003) Characterization of YqjM, an Old Yellow Enzyme homolog from *Bacillus subtilis* involved in the oxidative stress response. *J. Biol. Chem.* 278, 19891–19897.
- Blehert, D. S., Knoke, K. L., Fox, B. G., and Chambliss, G. H. (1997) Regioselectivity of nitroglycerin denitration by flavoprotein nitroester reductases purified from two *Pseudomonas* species. *J. Bacteriol.* 179, 6912–6920.
- Snape, J. R., Walkley, N. A., Morby, A. P., Nicklin, S., and White, G. F. (1997) Purification, properties, and sequence of glycerol trinitrate reductase from *Agrobacterium radiobacter*. *J. Bacteriol.* 179, 7796–7802.
- Miura, K., Tomioka, Y., Suzuki, H., Yonezawa, M., Hishinuma, T., and Mizugaki, M. (1997) Molecular cloning of the *nema* gene encoding N-ethylmaleimide reductase from *Escherichia coli*. *Biol. Pharm. Bull.* 20, 110–112.
- French, C. E., and Bruce, N. C. (1994) Purification and characterization of morphinone reductase from *Pseudomonas putida* M10. *Biochem. J.* 301 (Part 1), 97–103.
- Rohde, B. H., Schmid, R., and Ullrich, M. S. (1999) Thermoregulated expression and characterization of an NAD(P)H-dependent 2-cyclohexen-1-one reductase in the plant pathogenic bacterium *Pseudomonas syringae* pv. *glycinea*. *J. Bacteriol.* 181, 814–822.
- Blehert, D. S., Fox, B. G., and Chambliss, G. H. (1999) Cloning and sequence analysis of two *Pseudomonas* flavoprotein xenobiotic reductases. *J. Bacteriol.* 181, 6254–6263.
- Fetzner, S., Tshisuaka, B., Lingens, F., Kappl, R., and Hüttermann, J. (1998) Bacterial degradation of quinoline and derivatives: Pathways and their biocatalysts. *Angew. Chem., Int. Ed.* 37, 577–597.
- Griese, J. J., Jakob, R. P., Schwarzinger, S., and Dobbek, H. (2006) Xenobiotic reductase A in the degradation of quinoline by *Pseudomonas putida* 86: Physiological function, structure and mechanism of 8-hydroxycoumarin reduction. *J. Mol. Biol.* 361, 140–152.
- Kitzing, K., Fitzpatrick, T. B., Wilken, C., Sawa, J., Bourenkov, G. P., Macheroux, P., and Clausen, T. (2005) The 1.3 Å crystal structure of the flavoprotein YqjM reveals a novel class of Old Yellow Enzymes. *J. Biol. Chem.* 280, 27904–27913.
- Niino, Y. S., Chakraborty, S., Brown, B. J., and Massey, V. (1995) A new old yellow enzyme of *Saccharomyces cerevisiae*. *J. Biol. Chem.* 270, 1983–1991.
- Brige, A., Van den Hemel, D., Carpentier, W., De Smet, L., and Van Beuemen, J. J. (2006) Comparative characterization and expression analysis of the four Old Yellow Enzyme homologues from *Shewanella*

- oneidensis* indicate differences in physiological function. *Biochem. J.* 394, 335–344.
14. van Dillewijn, P., Wittich, R. M., Caballero, A., and Ramos, J. L. (2008) Subfunctionality of Hydride Transferases of the Old Yellow Enzyme Family of Flavoproteins of *Pseudomonas putida*. *Appl. Environ. Microbiol.* 74, 6703–6708.
 15. Williams, R. E., and Bruce, N. C. (2002) 'New uses for an Old Enzyme': The Old Yellow Enzyme family of flavoenzymes. *Microbiology* 148, 1607–1614.
 16. Abramovitz, A. S., and Massey, V. (1976) Interaction of phenols with old yellow enzyme. Physical evidence for charge-transfer complexes. *J. Biol. Chem.* 251, 5327–5336.
 17. Fox, K. M., and Karplus, P. A. (1994) Old yellow enzyme at 2 Å resolution: Overall structure, ligand binding, and comparison with related flavoproteins. *Structure* 2, 1089–1105.
 18. Karplus, P. A., Fox, K. M., and Massey, V. (1995) Flavoprotein structure and mechanism. 8. Structure-function relations for old yellow enzyme. *FASEB J.* 9, 1518–1526.
 19. Kohli, R. M., and Massey, V. (1998) The oxidative half-reaction of Old Yellow Enzyme. The role of tyrosine 196. *J. Biol. Chem.* 273, 32763–32770.
 20. Brown, B. J., Deng, Z., Karplus, P. A., and Massey, V. (1998) On the active site of Old Yellow Enzyme. Role of histidine 191 and asparagine 194. *J. Biol. Chem.* 273, 32753–32762.
 21. Xu, D., Kohli, R. M., and Massey, V. (1999) The role of threonine 37 in flavin reactivity of the old yellow enzyme. *Proc. Natl. Acad. Sci. U. S. A.* 96, 3556–3561.
 22. Fox, K. M., and Karplus, P. A. (1999) The flavin environment in old yellow enzyme. An evaluation of insights from spectroscopic and artificial flavin studies. *J. Biol. Chem.* 274, 9357–9362.
 23. Brown, B. J., Hyun, J. W., Duvvuri, S., Karplus, P. A., and Massey, V. (2002) The role of glutamine 114 in old yellow enzyme. *J. Biol. Chem.* 277, 2138–2145.
 24. Craig, D. H., Moody, P. C., Bruce, N. C., and Scrutton, N. S. (1998) Reductive and oxidative half-reactions of morphinone reductase from *Pseudomonas putida* M10: A kinetic and thermodynamic analysis. *Biochemistry* 37, 7598–7607.
 25. Barna, T., Messiha, H. L., Petosa, C., Bruce, N. C., Scrutton, N. S., and Moody, P. C. (2002) Crystal structure of bacterial morphinone reductase and properties of the C191A mutant enzyme. *J. Biol. Chem.* 277, 30976–30983.
 26. Messiha, H. L., Bruce, N. C., Sattelle, B. M., Sutcliffe, M. J., Munro, A. W., and Scrutton, N. S. (2005) Role of active site residues and solvent in proton transfer and the modulation of flavin reduction potential in bacterial morphinone reductase. *J. Biol. Chem.* 280, 27103–27110.
 27. Pudney, C. R., Hay, S., Pang, J., Costello, C., Leys, D., Sutcliffe, M. J., and Scrutton, N. S. (2007) Mutagenesis of morphinone reductase induces multiple reactive configurations and identifies potential ambiguity in kinetic analysis of enzyme tunneling mechanisms. *J. Am. Chem. Soc.* 129, 13949–13956.
 28. Barna, T. M., Khan, H., Bruce, N. C., Barsukov, I., Scrutton, N. S., and Moody, P. C. (2001) Crystal structure of pentaerythritol tetranitrate reductase: "Flipped" binding geometries for steroid substrates in different redox states of the enzyme. *J. Mol. Biol.* 310, 433–447.
 29. Khan, H., Harris, R. J., Barna, T., Craig, D. H., Bruce, N. C., Munro, A. W., Moody, P. C., and Scrutton, N. S. (2002) Kinetic and structural basis of reactivity of pentaerythritol tetranitrate reductase with NADPH, 2-cyclohexenone, nitroesters, and nitroaromatic explosives. *J. Biol. Chem.* 277, 21906–21912.
 30. Khan, H., Barna, T., Harris, R. J., Bruce, N. C., Barsukov, I., Munro, A. W., Moody, P. C., and Scrutton, N. S. (2004) Atomic resolution structures and solution behavior of enzyme-substrate complexes of *Enterobacter cloacae* PB2 pentaerythritol tetranitrate reductase. Multiple conformational states and implications for the mechanism of nitroaromatic explosive degradation. *J. Biol. Chem.* 279, 30563–30572.
 31. Khan, H., Barna, T., Bruce, N. C., Munro, A. W., Leys, D., and Scrutton, N. S. (2005) Proton transfer in the oxidative half-reaction of pentaerythritol tetranitrate reductase. Structure of the reduced enzyme-progesterone complex and the roles of residues Tyr186, His181, His184. *FEBS J.* 272, 4660–4671.
 32. Breithaupt, C., Kurzbauer, R., Lilie, H., Schaller, A., Strassner, J., Huber, R., Macheroux, P., and Clausen, T. (2006) Crystal structure of 12-oxophytodienoate reductase 3 from tomato: Self-inhibition by dimerization. *Proc. Natl. Acad. Sci. U.S.A.* 103, 14337–14342.
 33. Breithaupt, C., Strassner, J., Breiting, U., Huber, R., Macheroux, P., Schaller, A., and Clausen, T. (2001) X-ray structure of 12-oxophytodienoate reductase 1 provides structural insight into substrate binding and specificity within the family of OYE. *Structure* 9, 419–429.
 34. Fitzpatrick, T. B., Auweter, S., Kitzing, K., Clausen, T., Amrhein, N., and Macheroux, P. (2004) Structural and functional impairment of an Old Yellow Enzyme homologue upon affinity tag incorporation. *Protein Expression Purif.* 36, 280–291.
 35. Sambrook, J., and Russel, D. (2001) *Molecular Cloning: A Laboratory Manual*, Vol. 1, Cold Spring Harbor Laboratory Press, Plainview, NY.
 36. Aliverti, A., Curti, B., and Vanoni, M. A. (1999) Identifying and quantitating FAD and FMN in simple and in iron-sulfur-containing flavoproteins. *Methods Mol. Biol.* 131, 9–23.
 37. Massey, V., Stankovich, M., and Hemmerich, P. (1978) Light-mediated reduction of flavoproteins with flavins as catalysts. *Biochemistry* 17, 1–8.
 38. Sucharitakul, J., Chaiyen, P., Entsch, B., and Ballou, D. P. (2005) The reductase of p-hydroxyphenylacetate 3-hydroxylase from *Acinetobacter baumannii* requires p-hydroxyphenylacetate for effective catalysis. *Biochemistry* 44, 10434–10442.
 39. Loach, P. A. (1973) Oxidation-reduction potentials: Absorbance bands and molar absorbance of compounds used in biochemical studies. In *Handbook of Biochemistry Selected Data for Molecular Biology* (Sorber, H. A., Ed.) pp J33–J40, CRC Press, Cleveland, OH.
 40. Segel, I. H. (1993) *Enzyme Kinetics*, John Wiley and Sons, New York.
 41. Strickland, S., Palmer, G., and Massey, V. (1975) Determination of dissociation constants and specific rate constants of enzyme-substrate (or protein-ligand) interactions from rapid reaction kinetic data. *J. Biol. Chem.* 250, 4048–4052.
 42. Lang, P. T., Brozell, S. R., Mukherjee, S., Pettersen, E. F., Meng, E. C., Thomas, V., Rizzo, R. C., Case, D. A., James, T. L., and Kuntz, I. D. (2009) DOCK 6: Combining techniques to model RNA-small molecule complexes. *RNA* 15, 1219–1230.
 43. MacKerell, A. D. Jr., Banavali, N., and Foloppe, N. (2000) Development and current status of the CHARMM force field for nucleic acids. *Biopolymers* 56, 257–265.
 44. Brooks, B. R., Brooks, C. L. III, Mackerell, A. D. Jr., Nilsson, L., Petrella, R. J., Roux, B., Won, Y., Archontis, G., Bartels, C., Boresch, S., Caflisch, A., Caves, L., Cui, Q., Dinner, A. R., Feig, M., Fischer, S., Gao, J., Hodoscek, M., Im, W., Kuczera, K., Lazaridis, T., Ma, J., Ovchinnikov, V., Paci, E., Pastor, R. W., Post, C. B., Pu, J. Z., Schaefer, M., Tidor, B., Venable, R. M., Woodcock, H. L., Wu, X., Yang, W., York, D. M., and Karplus, M. (2009) CHARMM: The biomolecular simulation program. *J. Comput. Chem.* 30, 1545–1614.
 45. Bashford, D., and Karplus, M. (1990) pK_a's of ionizable groups in proteins: Atomic detail from a continuum electrostatic model. *Biochemistry* 29, 10219–10225.
 46. Messiha, H. L., Munro, A. W., Bruce, N. C., Barsukov, I., and Scrutton, N. S. (2005) Reaction of morphinone reductase with 2-cyclohexen-1-one and 1-nitrocyclohexene: Proton donation, ligand binding, and the role of residues Histidine 186 and Asparagine 189. *J. Biol. Chem.* 280, 10695–10709.
 47. Stewart, R. C., and Massey, V. (1985) Potentiometric studies of native and flavin-substituted Old Yellow Enzyme. *J. Biol. Chem.* 260, 13639–13647.
 48. DeLano, W. L. (2002) *The PyMol Molecular Graphics System*, DeLano Scientific, San Carlos, CA.